Photocatalytic Degradation of Ethylbenzene by Nano Photocatalyst in Aerogel form Based on Titania

Shirzad Taghanaki, Neda; Keramati, Narjes*[+]

Faculty of Nanotechnology, Semnan University, Semnan, I.R. IRAN

Mehdipour Ghazi, Mohsen

Faculty of Chemical, Petroleum and Gas Engineering, Semnan University, Semnan, I.R. IRAN

ABSTRACT: *In this study, a composite of Cu, N co-doped TiO_2@SiO_2 aerogel as a photocatalyst with enhanced optical absorption in the visible region as well as high specific surface area was synthesized by sol-gel method and ambient pressure drying process for degradation of Ethylbenzene. The physicochemical properties of the photocatalyst were examined by X-Ray Powder Diffraction, Scanning Electron Microscope, Photoluminescence, Fourier Transform Infrared Spectroscopy, Diffuse Reflectance Spectroscopy, Brouner Emmet Teller Isotherm/Barrett Joyner Halenda analysis. The structure of samples consisted of titanium dioxide crystalline phases in the dominant phase of the rutile and the amorphous structure of silica. The appearance of the Ti-O-Si peak confirmed the formation of TiO_2@SiO_2 composite. Based on the results of the characterization analysis, the type and concentration of dopants can be effective on the crystalline structure, bandgap energy, particle size, specific surface area, and the recombination of charge carriers. The sample contains 3 at. % of copper and nitrogen was able to degrade Ethylbenzene more efficiently in comparison with mono-doped TiO_2@SiO_2 nanocomposite under visible-light irradiation. The synergistic effects of Cu and N co-dopants were responsible for strong visible light absorption and effective separation of electron/hole.*

KEYWORDS: *Aerogel; Ethylbenzene; Photocatalyst; Visible light; Co-doped.*

INTRODUCTION

One of the challenges in chemical processes, in order to reduce environmental negative impacts, is the development of processes based on renewable energies such as sunlight [1]. TiO_2 (Titania) as the most studied photocatalyst, is a typical ultraviolet active semiconductor. This indicates that only a small fraction of the available solar spectrum (3–5%) has sufficient energy to drive TiO_2 photoexcitation [2, 3]. Hence, the sensitization of TiO_2 to active under visible light as the main part of the solar spectrum is a necessity [4]. On the other hand, regarding the fact that the reactions mainly occur on the surface of the photocatalysts, the specific surface area is one of the main factors that affect the activity of photocatalyst [5, 6].

Considerable efforts have been devoted to reduce

* *To whom correspondence should be addressed.*

+ E-mail: narjeskeramati@semnan.ac.ir

1021-9986/2021/2/525-537 13/$/6.03

the energy of the bandgap and create energy levels to promote electronic excitation into the visible light region [7-11]. Ion doping (either metal or non-metal) of TiO_2 is one of the most promising modification methods in this field [12-15]. At small quantities of dopant, as-produced impurity energy levels, not only cause redshift of the optical absorption edge to the visible light region but also act as trapping centers for electron–hole pairs, which is beneficial for enhancing the efficiency of photocatalytic reactions [16-19]. At higher concentration doping, it was experimentally observed that the impurity levels act as electron–hole pair recombination sites [20]. This is while reducing the bandgap by using low concentrations of doping is insufficient for the effective utilization of visible solar light [20]. More recently, the co-doping by non-metals in combination with transition metals as a novel approach to enhance synergistically the visible-light-driven photocatalytic activity of TiO_2 has attracted considerable interest [21-23].

Copper as one of the efficient transition metals impurities has a low price, non-toxicity and environmental acceptability [24]. Using Cu as co-dopants with various non-metals such as I, S and N have been studied for various photocatalytic applications [20]. Among non-metal elements, nitrogen offers several advantages due to its comparable atomic size with oxygen, high variety of precursors, stability and low cost [25, 26]. Experimental works on the co-doping of TiO_2 have shown a significantly better degradation rate of organic pollutants than the mono-doped TiO_2 under visible light irradiation [20, 27]. Increased photocatalytic activity in the visible light region regardless of the actual local arrangement of dopant atoms was also observed in theoretical work on the co-doping of TiO_2 anatase [23].

Furthermore, the activity of Titania is affected by its surface area. SiO_2 aerogel is stable and non-toxic support with high specific surface area and high porosity that can increase the available surfaces of the photocatalyst in adsorption of pollutant molecules and also improves the dispersion of TiO_2 particles [28-30]. The supercritical drying as a usual route for the production of silica aerogel requires high pressure, elevated temperature and special equipment to achieve these conditions. Hence, this method is considered unsafe and costly [31]. Accessibility of simple and safe synthetic approaches will incontrovertibly provide flexibility and hence intensify large-scale industrial production of aerogels. Ambient pressure drying which is carried out under low temperature and pressure is an efficient technology [32].

In this work, Cu, N co-doped TiO_2@SiO_2 aerogel photocatalysts active under visible light irradiation were synthesized by sol–gel technique followed by ambient pressure drying, using the cheapest industrial silica source (sodium silicate).

Ethylbenzene (EB) is widely used as a solvent (e.g., for organic synthesis and equipment cleaning) and also usually as a chemical raw material in numerous chemical productions [33]. Therefore, this material exists in petroleum products refinery and chemical industry wastewater. Due to improper waste disposal practices, accidental fuel spills and leaks in underground storage tanks and pipelines, EB is among the most common organic contaminants [34]. This pollutant has adverse effects on kidney, liver, blood and central nervous systems and International Agency for Research on Cancer (IARC) has classified EB as group 2B carcinogens [35, 36]. Adsorption systems has been identified as one of the most effective technologies for the removal and control the emission of VOCs such as benzene. However, adsorbents transfer pollutants to another media instead of destroying them. Another solution is bioremediation, which is a slow process and also has problems with activated sludge, including bulking. Mild operating conditions, lower operating costs, especially in the presence of visible light irradiation and higher degradation rate are the advantages of photocatalytic degradation over conventional treatment techniques.

In this study, the photocatalytic performance of synthesized Cu, N co-doped TiO_2@SiO_2 aerogel were tested in the photodegradation efficiency of ethylbenzene in aqueous media under visible light. The present work focuses on selecting the best molar concentration of dopant for co-doped TiO_2@SiO_2 visible light active aerogel photocatalyst and also comparing the activity of mono and co-doped photocatalysts.

EXPERIMENTAL SECTION

Materials

All chemical reagents were consumed as purchased from the manufacturer without further purification. Hexane (85% C_6H_{14}) and Methanol were purchased from Dr. Mojallali Industrial Chemical Complex Co. (Iran).

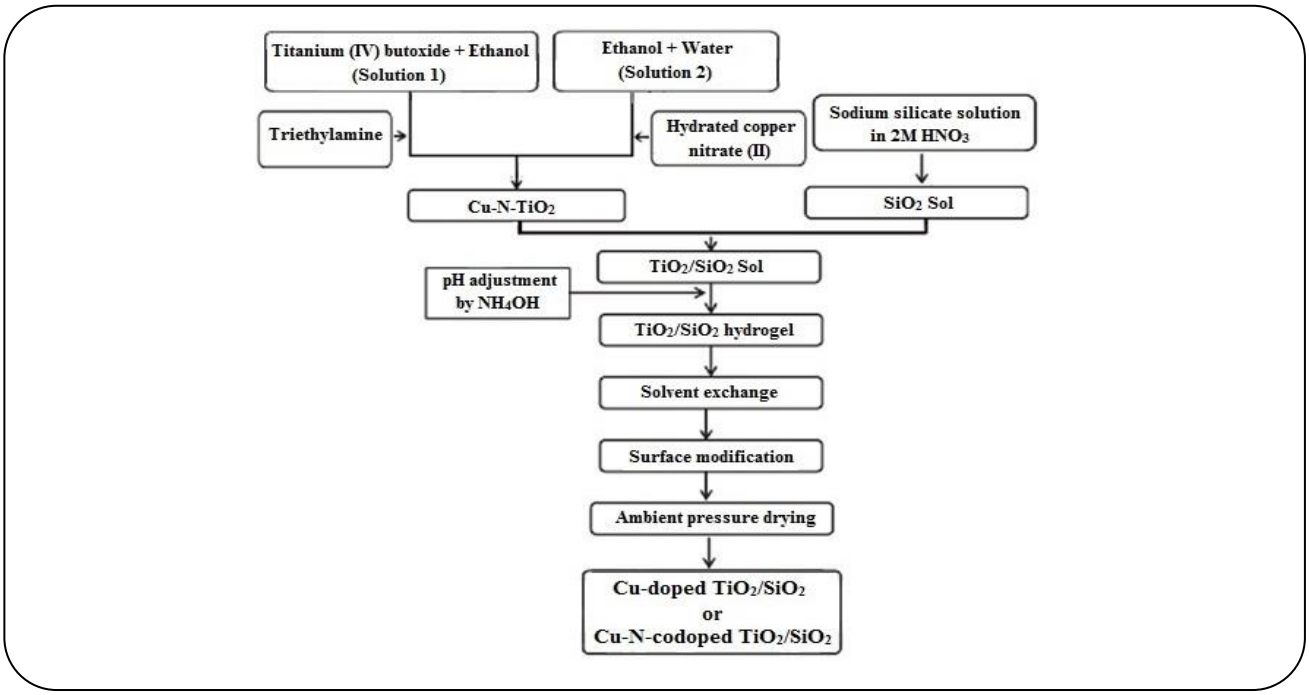

Scheme 1: A flow chart of the preparation method for Cu-N- co-doped TiO_2@SiO_2 aerogel nanocomposites.

Absolute Ethanol was obtained from Zakaria Jahrom Co. (Iran). Nitric acid (65% HNO_3) was bought from Kian Kaveh Azma Pharmaceutical Chemicals Complex Ltd. (Iran). Ammonium hydroxide solution (25% NH_4OH), Sodium silicate solution (SiO_2/Na_2O=3.24), Trimethylchlorosilane (TMCS) (C_3H_9SiCl), Titanium (IV) butoxide (Ti $(OCH_2CH_2CH_2CH_3)_4$), Triethylamine (N $(CH_2CH_3)_3$) and Hydrated copper nitrate (II) (Cu $(NO_3)_2.3H_2O$) were purchased from Merck Co. (Germany). Double distilled water was used for the preparation of the photocatalyst.

Preparation of photocatalysts

The Cu, N co-doped TiO_2@SiO_2 aerogel composite was prepared using sodium silicate and titanium (IV) butoxide as Si and Ti precursors, respectively according to literature with some modifications [20, 37]. A flow chart of the preparation process is shown in Scheme 1.

Initially, synthesis and characterization of Cu-doped specimens (mono doped TiO_2@SiO_2) were performed. After determining the best molar concentration of copper, co-doped samples were also prepared and studied. In a typical run, titanium (IV) butoxide was added to absolute ethanol at a molar ratio of 1:14 and mixed for 1h using a magnetic stirrer to form a homogeneous mixture (Solution 1). Similarly, a mixture of absolute ethanol and de-ionized water at a molar ration of 1:5 was prepared (solution 2). To prepare Cu doped TiO_2, hydrated copper nitrate (II) was dissolved in Solution 2, while for N doped TiO_2, triethylamine (N $(CH_2CH_3)_3$) was mixed with Solution 1. Afterward, solution of water–alcohol was added dropwise into alkoxide solution under constant stirring about 60 min. To enhance the homogeneity, the mixture was further stirred for 1h at room temperature.

Simultaneously, after adding 11.85 ml sodium silicate solution into de-ionized water at a volume ratio of 1:1 under constant stirring for 15 min and further stirring for 10 min, the resulting solution was added to 50 mL of 2M HNO_3 and mixed for 30min. The strong acidic sodium silicate solution was added into the preformed TiO_2 sol under vigorous stirring for 30 min. The pH of TiO_2@SiO_2 sol was adjusted to ~3.5 by dropwise addition of ammonium hydroxide solution in order to form a strong solid gel which was aged at 70 ℃ for 2 h and kept in the oven for 12 h to slowly reach its temperature to ambient temperature. After washing the gel by hexane to remove Na^+ ions, the solid gel was placed in ethanol for 12 h. The hydrogels were removed from ethanol and placed in a hexane/TMCS (20 vol %) mixture for further solvent exchange and surface modification for 6 h.

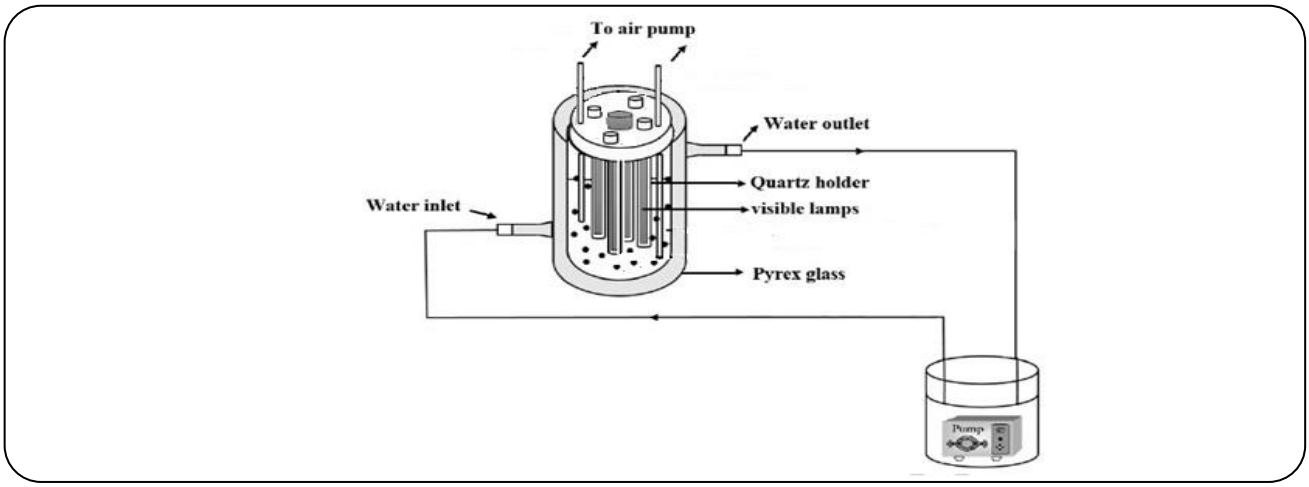

Fig. 1: Schematic diagram of the circular type photocatalytic reactor system.

The alcogels were removed from the mixture, washed with hexane and then dried at 80 ℃ for 3 h and heat-treated at 400 ℃ for 1.5 h. In this study, TiO_2 was doped with Cu and N using three different concentrations (1, 3 and 5 at. %) and these were dubbed the "atomic percent of Cu-atomic percent of N-TiO_2@SiO_2"; for example, the sample with 3 at. % of Cu and 3 at. % of N was labeled 3Cu-3N-TiO_2@SiO_2.

Photocatalytic experiments

Photocatalytic degradation of EB aqueous solution (50 ppm) was carried out in homemade Pyrex photoreactor under visible light irradiation using 0.4 g of photocatalyst at neutral pH (Fig. 1). Four quartz tubes, symmetrically embedded along the axis of the reactor, were used as pods to hold visible lamps (Philips, 60 W). The temperature was controlled through a cooling jacket around the reactor in the range of 20-25 °C. Injection of air into the reactor was carried out using an aquarium pump in order to provide the dissolved oxygen needed to carry out the photodegradation process and create mixing conditions to achieve uniform photocatalyst distribution. Since ethylbenzene is a volatile material, therefore, during the degradation process, all seams of the reactor were blocked and the maximum volume of reactor was used to prepare the sample contaminant solution.

Prior to irradiation, the powder suspension was stirred for 60 min under a constant rate of aeration in the darkness, until adsorption/desorption equilibrium was reached. Then, 10 ml samples were taken from the reactor at different intervals. In order to prevent the catalyst interfering with the reading of the spectrophotometer, samples were first centrifuged and the supernatant was analyzed using a UV–Vis spectrophotometer. With purpose minimizing the possibility of evaporation at this stage, all the volumes of the falcons were completely filled with solution and their lids tightened and insulated around the lid. There was no significant change in the mass of photocatalysts, where the photocatalyst was collected after each use of the reactor and used again for subsequent testing. In other words, the amount of particles in the treated solution was low.

The photodegradation of EB was monitored *via* its normalized intensity of the absorption band at around $\lambda_{max} = 250$ nm based on Eq. (1), where C_0 and C_t are initial and final EB concentration (after 90 min irradiation), respectively:

$$\%\text{Degradation}=[(C_0-C_t)/C_0]*100 \quad (1)$$

Prior to photocatalytic experiments, a test was performed similar to the photocatalytic degradation test, but without adding photocatalyst, to ensure that EB photolysis does not occur under visible light exposure. Based on the data obtained from the UV-Vis absorption spectra, the change in the concentration of EB was negligible.

A series of controlled experiments using radical scavengers were carried out to understand the probable reaction mechanism for the photocatalytic degradation of EB over synthesized photocatalyst. Two sacrificial agents were added to reactor for removing the corresponding active species, methanol (MeOH) for removing $^{\bullet}OH$ and ethanol (EtOH) as e^- scavenger.

Characterization

The crystal structures were characterized via X-Ray Diffraction (XRD) analysis (Bruker, D8) with Cu-Kα radiation (λ= 0.1546 nm). The specific surface area, average pore diameter and the structure of pores were derermined by the nitrogen physisorption isotherms, and Brunauer-Emmett-Teller and Barrett-Joyner-Halenda (BET-BJH) analyses (Belsorp, mini II). The UV–Vis absorption spectra were recorded using a UV–Vis spectrophotometer (Shimadzu, UV-1650PC). Photoluminescence (PL) study was carried out using a fluorescence spectrophotometer (Varian; Cary eclipse). The Diffusive reflectance Spectra (DRS) of the samples were recorded by a UV–Vis Spectrophotometer (Avantes, Avaspec 2048 TEC). The structures of the aerogels were observed with a scanning electron microscope (VEGA; TESCAN-XMU). A Fourier transform infrared Spectrometer (Shimadzu, 8400 S) was used to determine the functional groups of the photocatalysts.

RESULTS AND DISCUSSION

Cu mono doped TiO_2@SiO_2 composite

In order to determine the best concentration of copper in mono doped composite, Cu-TiO_2@SiO_2 using three different concentrations of Cu were prepared. According to the X-ray diffraction patterns (Fig. 2), Cu-TiO_2@SiO_2 photocatalysts consisted of both crystalline and amorphous phases. The hump in the range from 15° to 30° suggests the presence of amorphous SiO_2 [38]. The crystallite size calculated from the Debye–Sherrer equation using the prominent peak of anatase (101) and rutile (110) phases and phase fraction determined by the Spurr and Myers equation is presented in Table 1.

Results indicated that rutile was the predominant crystalline phase in synthesized samples. As can be seen, acidic pH of the reaction medium provided conditions for the formation of a rutile phase in ambient temperature as a predominant phase. According to the Cu-precursor (Hydrated Copper (II) nitrate), Cu^{2+} should be formed in the solution. According to results, increasing the concentration of copper from 1 to 3 at. %, the crystallite size was increased. As the Cu dopant concentration increased from 1 to 3 at%, the W_R and crystallite size also increased. Increasing the crystallite size could indicate an improvement in the crystallinity of the sample structure. However, by reaching the amount of copper up to 5 at. %, the crystallite size, and W_R were reduced. Cu^{2+} can replace Ti^{4+} in the substitutional sites or be incorporated in the interstitial sites. In some cases, it may separately accumulate on the surface of TiO_2 [39].

Munir et al. [40] have described that at low dopant concentrations, the prominent substitutional doping increases the crystallinity of the sample. However, at a high amount of dopant, interstitial doping predominates the substitutional doping. On the other hand, the substitution of Ti^{4+} by Cu^{2+} increases the oxygen vacancy concentration which is responsible for anatase to rutile phase transition [39]. So it is possible that increasing dominant substitution doping by increasing the amount of copper from 1 to 3 at% leads to an increase in W_R and crystallite size. Whereas with increasing concentration of copper from 3 to 5%, interstitial doping predominates the substitutional doping, and hence the conversion of phase from anatase to rutile has been less. Also, the accumulation of excess copper ions near the boundary can prevent the growth of crystals [27].

Optical properties of Cu-TiO_2@SiO_2 were studied by measuring optical spectra in diffuse reflectance mode. Tauc plot is presented in Fig. 3 which was used to evaluate the bandgap energy of synthesized photocatalysts. With increasing Cu concentration from 1 to 3 at%, the bandgap was shifted from 2.9 to 2.82 eV. By reducing the band gap of semiconductors, a larger number of charge carriers can be formed which in turn can improve the degradation efficiency of the photocatalysts.

With increasing the concentration of Cu up to 5 at%, the bandgap was blue-shifted to 2.86 eV. The blue shift in the absorption spectra can be explained by the Burstein-Moss (BM) effect [41]. When the dopant concentration increases from a certain value, the excess amount of the charge carries causes the Fermi level lying inside the conduction band. Thereafter, the additional exciting electrons can only be excited into the conduction band above the Fermi level. This Condition leads to the widening of the semiconductor bandgap [40, 42].

Data related to the weight fraction of the rutile phase, bandgap and EB photodegradation efficiency by Cu-TiO_2@SiO_2 samples are summarized in Table 1. A comparison of obtained values shows that the best degradation efficiency was obtained in the presence of 3Cu-TiO_2@SiO_2 photocatalyst which has the smallest bandgap and the highest

Table 1: Effect of Concentration of dopant in mono doped TiO_2@SiO_2 aerogel on EB photodegradation.

Sample name	W_R	Crystallite size (nm)		Bandgap (eV)	EB degradation efficiency (%)
		Anatase	Rutile		
1Cu-TiO_2@SiO_2	0.658	21.21	18.23	2.90	65
3Cu-TiO_2@SiO_2	0.792	21.22	31.94	2.82	78
5Cu-TiO_2@SiO_2	0.720	18.18	17.08	2.86	35

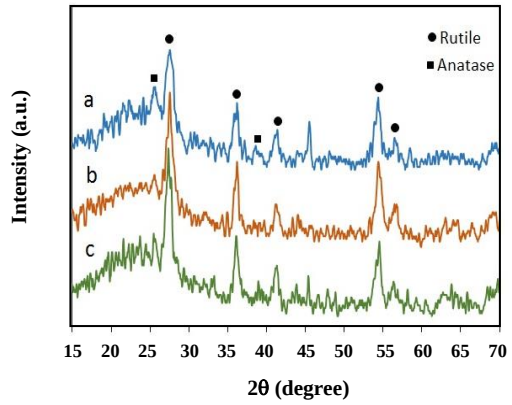

Fig. 2: XRD patterns of a) 1Cu-TiO_2@SiO_2 b) 3Cu-TiO_2@SiO_2 and c) 5Cu-TiO_2@SiO_2 samples.

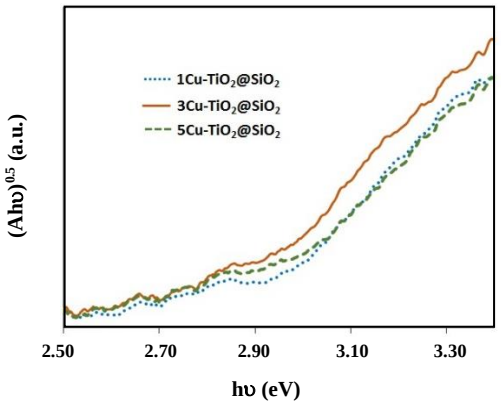

Fig. 3: Tauc plot of Cu-TiO_2@SiO_2 samples with three different concentrations of dopant.

weight fraction of rutile phase. The 5Cu-TiO_2@SiO_2 sample also has a smaller energy bandgap and a higher W_R than the 1Cu-TiO_2@SiO_2 sample. However, it was shown a weaker photocatalytic performance. As discussed already, the dopant concentrations play an important role in photocatalytic activity. At higher molar concentration, these impurities themselves increase the charge carrier recombination. Thus, the presence of larger amounts of copper can reduce the degradation efficiency of the 5Cu-TiO_2@SiO_2 sample through reducing the lifetime of photogenerated electron/hole pairs. On the basis of these results, 3 at. % of Cu was selected for the synthesis of co-doped TiO_2@SiO_2 samples in the next section.

Cu, N co-doped TiO_2@SiO_2 composite

According to the XRD patterns of co-doped TiO_2@SiO_2 samples presented in Fig. 4 as well as, the information provided in Table 2, with increasing the amount of nitrogen up to 3 and 5%, the main anatase peak removed from the XRD patterns. In this research, Cu $(NO_3)_2$ has been used as a source of copper, so Cu^{2+} is formed in the reaction medium. On the other hand, based on the truth of the Hume-Rothery rules in relation to the copper and titanium ionic radius, this is most probably that Cu^{2+} dissolves into TiO_2 crystal lattice [43]. However, the relatively small difference between the ionic radius of Cu^{2+} (0.086 nm) and Ti^{4+} (0.0745 nm) can cause the variation in the lattice dimension of TiO_2 [44]. In addition, the replacement of oxygen with nitrogen atoms creates oxygen deficiency in TiO_2 lattice. The simultaneous presence of both these features in co-doped samples allows the rearrangement of Ti^{4+} and O_2^- ions in the TiO_2 lattice to favor the anatase to rutile phase transformation [20].

Fig. 5 shows the Tauc plot of co-doped samples. The results indicated that the addition of N dopant from 1 to 3 at. % narrowed the bandgap of composite from 2.71 to 2.6 eV. However, increasing the amount of nitrogen up to 5 at. % resulted in a blue shift in the energy gap (2.68 eV) of the photocatalyst. Valentin et al. [45] demonstrated that due to different structures and densities, high levels of N-doping have opposite effects on the photoactivity of anatase and rutile, leading to a redshift and a blue shift, respectively, of the absorption band edge. In both polymorphs, the doping is accompanied by the appearance of N 2p localized states just above the top of the O 2p

Table 2: Effect of Concentration of dopant in codoped TiO_2@SiO_2 aerogel on EB degradation.

Sample name	W_R	Crystallite size (nm)		Bandgap (eV)	EB degradation efficiency (%)
		Anatase	Rutile		
3Cu-1N-TiO_2@SiO_2	0.84	12	31.90	2.71	82
3Cu-3N-TiO_2@SiO_2	1	---	31.93	2.60	90
3Cu-5N-TiO_2@SiO_2	1	---	30	2.68	70

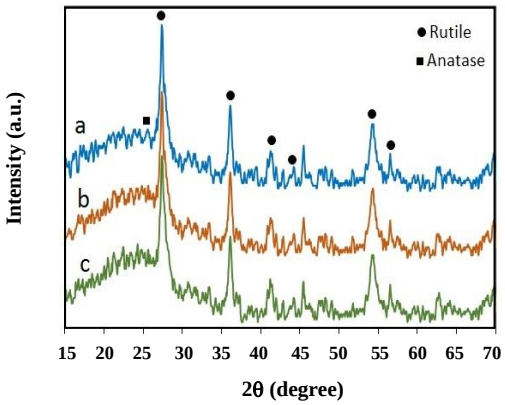

Fig. 4: XRD patterns of a) 3Cu-1N-TiO_2@SiO_2 b) 3Cu-3N-TiO_2@SiO_2 and c) 3Cu-5N-TiO_2@SiO_2 samples.

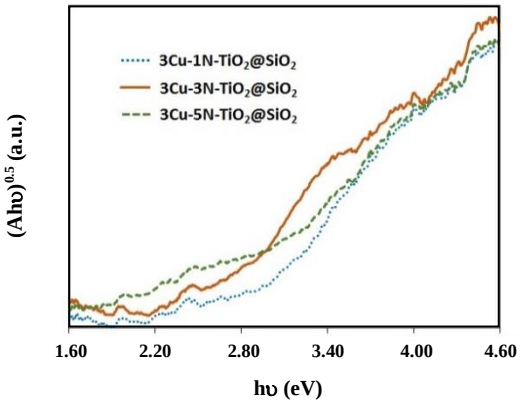

Fig. 5: Tauc plot of Cu, N co-doped TiO_2@SiO_2 samples.

valence bond, but in rutile, the shift of the top of the valence band towards lower energies leads to an overall increase of the optical transition energy [46].

Photocatalytic activities of co-doped TiO_2@SiO_2 samples under visible light irradiation were also determined. Among them, 3Cu-3N-TiO_2@SiO_2 which compared with the other two samples has the narrowest band gap and more weight fraction of the rutile phase than the 3Cu-1N-TiO_2@SiO_2 (Table 2), exhibited the highest photocatalytic activity (90%). The 3Cu-5N-TiO_2@SiO_2 sample also has a higher W_R and a narrower bandgap energy than the 3Cu-1N-TiO_2@SiO_2 specimen.

However, 3Cu-1N-TiO_2@SiO_2 had a better photocatalyst performance. Chemical absorption of nitrogen on the 3Cu-5N-TiO_2@SiO_2 surface may cause a decrease in its photocatalytic activity. Because increasing the molar concentration of nitrogen can cause its chemical absorption at the photocatalyst surface. Absorbed nitrogen on the surface, covers the surface of the sample and reduces the number of active sites available for pollutant molecules, water and oxygen and, consequently, decreases the photocatalytic degradation efficiency [28, 47]. Therefore, the dopant concentrations of 3 at. % for Cu and 3 at. % for N was selected for co-doping of TiO_2@SiO_2 as the best molar concentrations.

Comparison of optimum mono and co-doped TiO_2@SiO_2

Fig. 6 indicates the curves of nitrogen adsorption-desorption and the pore size distribution diagrams for two optimum mono and co-doped nanophotocatalysts. One of the goals of this work was to produce a photocatalyst at ambient pressure with a high specific surface area. The BET surface area for 3Cu–3N–TiO_2@SiO_2 and 3Cu–TiO_2@SiO_2 were 493.87 and 469.76 m^2/g, respectively.

The N_2 adsorption-desorption isotherms displayed a type IV isotherm with a type H1 hysteresis loop [48]. The Type IV isotherm is a good indication of the mesoporosity of these samples and the presence of H1 type depicted the presence of cylindrical pores [48]. Average pore diameter about 4.8-5.2 nm was obtained by the curves of pore size distributions, which were plotted using data estimated by BJH method. Continuous condensation of end –OH groups during the wet gel drying under ambient pressure can be prevented by solvent exchange and surface modification. Solvent exchange process was performed by placing the solid gel in ethanol to eliminate remaining water from the pores. Reductions

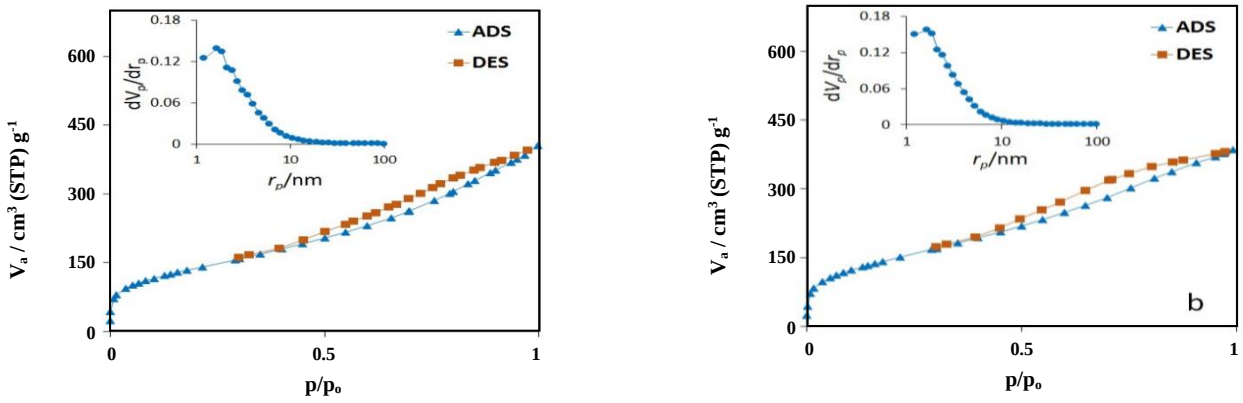

Fig. 6: N_2 adsorption-desorption isotherms and pore size distribution of a) 3Cu-TiO_2@SiO_2 and b) 3Cu-3N-TiO_2@SiO_2 samples.

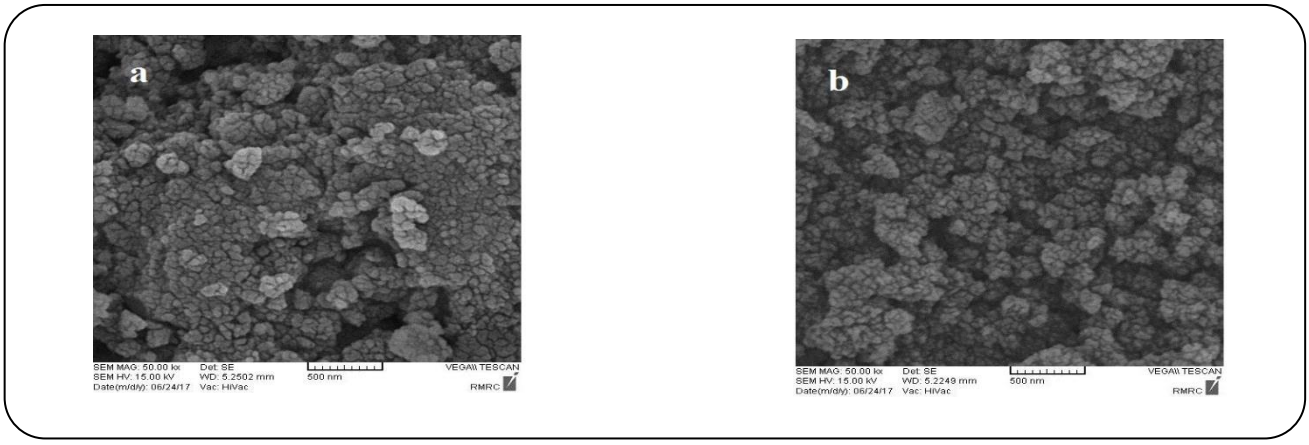

Fig. 7: SEM images of a) 3Cu-TiO_2@SiO_2 and b) 3Cu-3N-TiO_2@SiO_2 samples

of surface tension can be done by replacing the hydrophilic –OH groups on the surface of the gel backbone with unreactive Si–CH_3 species using silane coupling agents (TMCS and hexane). A comparison of the obtained surface area indicated that the nitrogen dopant had a positive effect on the increase of the specific surface area. A similar result has been reported in previous studies [20, 49].

The structure of 3Cu–3N–TiO_2@SiO_2 and 3Cu–TiO_2@SiO_2 were investigated by SEM and depicted in Fig. 7. This figure revealed that the particle aggregation in the 3Cu-3N-TiO_2@SiO_2 sample with an average particle size of ~38.07 nm was less than that of 3Cu-TiO_2@SiO_2 with an average particle size of ~47.25 nm. Triethylamine is a tridentate ligand that forms a stable complex with titanium. This complex plays an important role in the stability of nanoparticles and prevents their growth and aggregation. This may be the reason for the particle size reduction of 3Cu-3N-TiO_2@SiO_2 compared to another [48, 49]. As a result of the particle size change, the size of the crystallites is also affected as seen in the XRD analysis results, which the size of rutile phases in optimum co-doped sample was smaller than mono-dope.

The PL measurements have been widely employed in order to investigate the efficiency of charge carrier trapping, migration, transfer, and separation of electron–hole pairs in semiconductor particles, since PL signals in TiO_2 originate from the radiative recombination of photogenerated charges [20, 50]. Fig. 8 shows the emission peaks in violet (420 nm), blue (485 nm) and green (528) regions for both, mono-doped and co-doped samples. The peak observed at 420 nm occurs by band-to-band recombination through the transition along the band edge [51]. The second and third peaks originate from the intraband transitions within the energy level traps or surface defects [20, 52]. According to the signals, the intensity of these peaks for 3Cu-3N-TiO_2@SiO_2

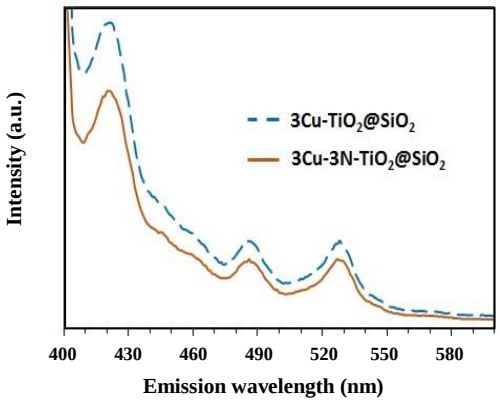

Fig. 8: Photoluminescence emission spectra of 3Cu-TiO₂@SiO₂ and 3Cu-3N-TiO₂@SiO₂ samples.

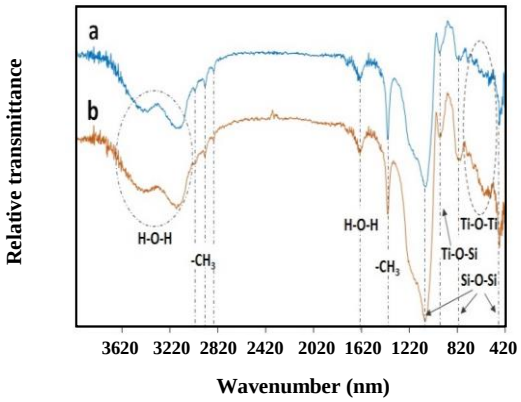

Fig. 9: FTIR spectra of a) 3Cu-TiO₂@SiO₂ and b) 3Cu-3N-TiO₂@SiO₂ samples.

has been reduced compared with the sample without nitrogen. Reducing the recombination rate improves the photocatalytic activity since in this case, more photogenerated charge carriers can participate in the photocatalytic degradation process [53]. This result is in good agreement with the result of the photodegradation of EB by these composites.

The 3Cu-TiO_2@SiO_2 and 3Cu-3N-TiO_2@SiO_2 samples were further investigated with FT-IR spectra shown in Fig. 9. The absorption peaks in the region wavenumber of 500-700 cm^{-1} correspond to the stretching vibration of Ti-O-Ti [54]. The absorption bands assignable to rocking vibration, symmetrical and asymmetrical stretching vibration of Si–O–Si can be seen at 468 cm^{-1}, 780–815 cm^{-1} and 1080–1090 cm^{-1}, respectively [37, 49, 55]. The existence of the peak at 950-960 cm^{-1} corresponds to the vibration of hetero-linkage Ti–O–Si bond indicates the incorporation of TiO_2 into SiO_2 to form binary SiO_2–TiO_2 systems [56-58]. The absorption peaks at 3000–3740 cm^{-1} and 1524–1691 cm^{-1} assigned to the hydroxyl groups as a result of physically adsorbed water by the composite aerogel photocatalysts [37, 58, 59].

The absence of absorption bands corresponding to Si-CH_3 groups in the spectra of synthetic samples may be due to the thermal decomposition of methyl groups and the formation of hydroxyl groups during the thermal process around 400 ° C [60]. However, the peaks at 2850–2975 cm^{-1} and 1400 cm^{-1} attributable to C–H groups which in some cases are stable up to 800 ° C which is inevitable [5, 37].

In a heterogeneous photocatalytic process, degradation of organic pollutants such as EB occurs by reacting the adsorbed pollutants on the surface of the photocatalyst with oxidizing agents (O_2•$^-$ and OH• radicals) produced by photogenerated charge carriers in photocatalyst from absorbed O_2 and H_2O [17]. Therefore main factors, including surface area, bandgap of the photocatalyst, the separation efficiency of electron–hole pairs and also which are of effective parameters for the efficient degradation reaction. High surface area can be effective in increasing the absorption of the reactants on the active sites [20, 61]. Narrowing of the band gap can increases the efficiency in visible light photons absorption that contributes to the higher number production of charge carriers thus increasing the degradation rate of pollutants. Determining the best amount of dopant is important because at concentrations above this value the same trapping sites operate as the recombination centers. This can be a reason for reducing the photocatalytic activity at high concentrations of Cu and N doping in TiO_2@SiO_2 composite aerogel photocatalysts.

In other hands, the particle size of nanocrystalline photocatalysts plays an important role in the dynamics of the electron/hole recombination process. A decrease in particle size can improve the photonic efficiency through increasing the interfacial charge carrier transfer rate [62]. According to the explanations presented, it can be concluded that 3Cu-3N-TiO_2@SiO_2 shows higher photocatalytic activity for the degradation of EB as compared with the 3Cu-TiO_2@SiO_2 mainly due to the synergistic effects of reduced electron-hole recombination, higher specific surface area and reduced bandgap.

From the comparison of the degradation efficiency, it was observed that by addition of methanol to the photodegradation

process, the efficiency of EB degradation was decreased, indicating that the hydroxyl free radicals have played an important role in EB degradation by the synthesized photocatalyst.

Based on the absorption spectrum, the absorption peak of aromatic derivatives for none of the final solutions was observed. In addition, since the hydroxyl radical has been the major oxidizing agent in the degradation of ethylbenzene, it can be predicted that by attacking this radical on the benzene ring, the structure is degraded and converted to linear compounds. With the continuous hydroxylation of aromatic acids produced, followed by the opening of the benzene ring, acetic acid is produced. Also, further oxidation of aliphatic acids will produce water and carbon dioxide compounds. The results of several studies show that the production intermediates in photocatalytic degradation of various aromatic pollutants are related to the hydroxylation of benzene ring [63-65].

CONCLUSIONS

In this study, Cu-TiO_2@SiO_2 and Cu-N-TiO_2@SiO_2 aerogel photocatalyst powders using three different concentrations of Cu and N were synthesized by the sol-gel method *via* ambient pressure drying. The 3Cu-3N-TiO_2@SiO_2 showed the highest photocatalytic activity in the degradation of EB under visible light irradiation (90%). The samples consisted of both anatase and rutile phases but the acidic pH of the reaction medium leads to the formation of rutile as the predominant crystalline phase in ambient temperature. It was found that the addition of nitrogen and copper dopants into composite led to the phase transition from anatase to rutile. The results showed that the use of optimal concentration of copper and nitrogen dopants reduced the recombination rate of photogenerated charge carriers as compared to the mono doped samples. Using copper and nitrogen impurities, the bandgap of the photocatalyst was narrowed. The increased photocatalytic activity of the 3Cu-3N-TiO_2@SiO_2 photocatalyst can be attributed to the *smaller* bandgap, efficient separation of photoinduced charges, and a higher surface area. Experiments concerning radical scavengers indicated that the active radical of hydroxyl (•OH) in the solution was the main reactive species.

Received : Nov. 26, 2019 ; Accepted :May 4, 2020

REFERENCES

[1] Lang X., Chen X., Zhao J., Heterogeneous visible Light Photocatalysis for Selective Organic Transformations, *Chem. Soc. Rev.*, **43**: 473-486 (2014).

[2] Bahramian A. R., Enhanced Photocatalytic Activity of Sol-Gel Derived Coral-like TiO_2 nanostructured Thin Film, *Iran. J. Chem. Chem. Eng.*(IJCCE), **35**: 27-41 (2016).

[3] Zatloukalová K., Obalová L., Kočí K., Photocatalytic Degradation of Endocrine Disruptor Compounds in Water over Immobilized TiO_2 Photocatalysts, *Iran. J. Chem. Chem. Eng. (IJCCE)*, **36**: 29-38 (2017).

[4] Ahmadkhani R., Habibi-Yangjeh A., Facile ultrasonic-Assisted Preparation of Fe_3O_4/Ag_3VO_4 Nanocomposites as Magnetically Recoverable Visible-Light-Driven Photocatalysts with Considerable Activity, *J. Iran. Chem. Soc.*, **14**: 863 (2017).

[5] Zu G., Shen J., Wang W., Zou L., Lian Y., Zhang Z., Silica-Titania Composite Aerogel Photocatalysts by Chemical Liquid Deposition of Titania onto Nanoporous Silica Scaffolds, *Appl. Mater. Interfaces*, **7**: 5400–5409 (2015).

[6] Etacheri V., Roshan R., Kumar V., Mg-Doped ZnO Nanoparticles for Efficient Sunlight-Driven Photocatalysis, *Appl. Mater. Interfaces*, **4 (5)**: 2717-2725 (2012).

[7] Niu X., Yu J., Wang L., Fu C., Wang J., Wang L., Zhao H., Yang J., Enhanced Photocatalytic Performance of TiO2 Nanotube-Based Heterojunction Photocatalyst Via the Coupling of Grapheme and FTO, *Appl. Surf. Sci.*, **413**: 7–15 (2017).

[8] Meng A., Zhu B., Zhong B., Zhang L., Cheng B., Direct Z-Fig. TiO_2/CdS Hierarchical Photocatalyst For Enhanced Photocatalytic H_2-production Activity, *Appl. Surf. Sci.*, **422**: 518–527 (2017).

[9] Wang P., Lu Y., Wang X., Yu H., Co-modification of Amorphous-Ti(IV) Hole Cocatalyst and $Ni(OH)_2$ Electron cocatalyst for Enhanced Photocatalytic H_2-Production Performance of TiO_2, *Appl. Surf. Sci.*, **391**: 259–266 (2017).

[10] Wang X., Li T., Yu R., Yu H., Yu J., Highly Efficient TiO_2 Single-Crystal Photocatalyst with Spatially Separated Ag and F Bi-Cocatalysts: Orientation Transfer of Photogenerated Charges and their Rapid Interfacial Reaction, *J. Mater. Chem. A.*, **4**: 8682–8689 (2016).

[11] Pazhooh P., Khoshnavazi R., Bahrami L., Naseri E., Synthesis and Photocatalytic Activity Assessing of the TiO_2 nanocomposites Modified by Some Lanthanide Ions and Tin-Derivative Sandwich-Type Polyoxometalates, *J. Iran. Chem. Soc*., **1** (2018).

[12] Ramacharyulu P.V.R.K., Nimbalkar D.B., Kumar J.P., Prasad G.K., Chu Ke Sh., N-Doped, Si-Doped TiO_2 Nanocatalysts: Synthesis, Characterization and Photocatalytic Activity in the Presence of Sunlight, *RSC Adv*., **5**: 37096-37101 (2015).

[13] Pham T.D., Lee B.K., Lee Ch.H., The Advanced Removal of Benzene from Aerosols by Photocatalytic Oxidation and Adsorption of Cu–TiO_2/PU under Visible Light Irradiation, *Appl. Catal. B.*, **182**: 172–183 (2016).

[14] Cheng G., Xu F., Stadler F.J., Chen R., A facile and General Synthesis Strategy to Doped TiO_2 Nanoaggregates with Mesoporous Structure and Comparable Property, *RSC Adv*., **5**: 64293-64298 (2015).

[15] Hojat Ansari S., Giahi M., Photochemical Degradation of Fluocinolone Acetonidin Drug in Aqueous Solutions Using Nanophotocatalyst ZnO Doped by C, N, and S, *Iran. J. Chem. Chem. Eng. (IJCCE)*, **36**: 183-189 (2017).

[16] Dong H., Zeng G., Tang L., Fan C., Zhang C., He X., He Y., An Overview on Limitations of TiO_2-Based Particles for Photocatalytic Degradation of Organic Pollutants and the Corresponding Countermeasures, *Water Res.*, **79**: 128–146 (2015).

[17] Jaiswal R., Patel N., Kothari D.C., Miotello A., Improved Visible Light Photocatalytic Activity of TiO_2 co-Doped with Vanadium and Nitrogen, *Appl. Catal. B.*, **126**: 47–54 (2012).

[18] Gnanaprakasam A. J., Sivakumar V. M., Thirumarimurugan M., Investigation of Photocatalytic Activity of Nd-doped ZnO Nanoparticles Using Brilliant Green Dye: Synthesis and Characterization, *Iran. J. Chem. Chem. Eng. (IJCCE)*, **37**: 61-71 (2018).

[19] Habibi M.H., Bagheri P., Spinel Cobalt Manganese Oxide Nano-Composites Grown Hydrothermally on Nanosheets for Enhanced Photocatalytic Mineralization of Acid Black 1 Textile Dye: XRD, FTIR, FESEM, EDS and TOC studies, *J. Iran. Chem. Soc*., **14**: 1643 (2017).

[20] Jaiswal R., Bharambe J., Patel N., Alpa D., Kothari D.C., Miotello A., Copper and Nitrogen co-doped TiO_2 Photocatalyst with Enhanced Optical Absorption and Catalytic Activity, *Appl. Catal. B.*, **168**: 333–341 (2015).

[21] Rimoldi L., Ambrosi C., Di Liberto G., Lo Presti L., Ceotto M., Oliva C., Meroni D., Cappelli S., Cappelletti G., Soliveri G., Ardizzone S., Impregnation Versus Bulk Synthesis: How the Synthetic Route Affects the Photocatalytic Efficiency of Nb/Ta: N Co-doped TiO2 Nanomaterials, *J. Phys. Chem. C.*, **119 (42)**: 24104-24115 (2015).

[22] Bloh J.Z., Folli A., Macphee D.E., Adjusting Nitrogen Doping Level in Titanium Dioxide by Codoping with Tungsten: Properties and Band Structure of the Resulting Materials, *J. Phys. Chem. C*., **118 (36)**: 21281-21292 (2014).

[23] Koteski V., Belošević-Čavor J., Umićević A., Ivanovski V., Toprek D., Improving the Photocatalytic Properties of Anatase TiO_2 (101) Surface by co-doping with Cu and N: *Ab Initio* Study, *Appl. Surf. Sci*. **425**: 1095-1100 (2017).

[24] Tahir M., Tahir B., Dynamic Photocatalytic Reduction of CO_2 to CO in a Honeycomb Monolith Reactor Loaded with Cu and N Doped TiO_2 Nanocatalysts, *Appl. Surf. Sci*., **377**: 244–252 (2016).

[25] Cinthia G., Guevara A., Iliana E., Ramírez M., Hernández-Ramírez A., Jáuregui-Rincón J., Antonio Lozano-Álvarez J., Luis Rodríguez-López J., Comparison of Two Synthesis Methods on the Preparation of Fe, N-Co-doped TiO_2 Materials for Degradation of Pharmaceutical Compounds under Visible Light, *Ceram. Int*., **43 (6)**: 5068-5079 (2017).

[26] Taherinia M., Nasiri M., Abedini E., Pouretedal H.R., Comparing the Photocatalytic Activity of N-Doped And S-Doped Titanium Dioxide Nanoparticles for Water Splitting Under Sunlight Radiation, *J. Iran. Chem. Soc.*, **15**: 1301 (2018).

[27] Wang S., Yang X.J., Jiang Q., Lian J.S., Enhanced Optical Absorption And Photocatalytic Activity of Cu/N-Codoped TiO_2 Nanocrystals, *Mater. Sci. Semiconductor. Process*, **24**: 247–253 (2014).

[28] Pal A., Jana T.K., Chatterjee K., Silica Supported TiO_2 Nanostructures for Highly Efficient Photocatalytic Application Under Visible Light Irradiation, *Mater. Res. Bull*., **76**: 353–357 (2016).

[29] Zhu J., Xie J., Chen M., Jiang D., Wu D., Low-Temperature Synthesis of Anatase Rare Earth Doped Titania-Silica Photocatalyst and its Photocatalytic Activity under Solar-Light, *Colloids. Surf. A.: Physicochem. Eng. Aspects*, 355: 178–182 (2010).

[30] Jiang R., Zhu H.Y., Li J.B., Fu F.Q., Yao J., Liang X.X., Guo R.Q., Zeng G.M., Efficient Solar Photocatalyst Based on Ag3PO4/Graphene Nanosheets Composite for Photocatalytic Decolorization of Dye Pollutants, *J. Iran. Chem. Soc*., **13**: 1167 (2016).

[31] Young Lee K., Min Park S., Beom Kim J., El Saliby I., Shahid M., Kim G.J., Kyong Shon H., Kim J.H., Synthesis and Characterisation of Porous Titania-Silica Composite Aerogel for NOx and Acetaldehyde Removal, *J. Nanosci. Nanotechnol*., **16**: 4505–4511 (2016).

[32] Mermer N.K., Sari Yilmaz M., Dere Ozdemir O., Burcin Piskin M., The Synthesis of Silica-Based Aerogel from Gold Mine Waste for Thermal Insulation, *J. Therm. Anal. Calorim.*, **129 (2)**: 1807-1812 (2017).

[33] Powers S.E., Hunt C.S., Heermann S.E., Corseuil H.X., Rice D., Alvarez P.J.J., The Transport And Fate of Ethanol and BTEX in Groundwater Contaminated by Gasohol, *Crit. Rev. Environ. Sci. Technol.*, **31**: 79–123 (2001).

[34] Cui H., Gu X., Lu Sh., Fu X., Zhang X., Fu G.Y., Qiu Zh., Sui Q., Degradation of Ethylbenzene in Aqueous Solution by Sodium Percarbonate Activated with EDDS–Fe(III) Complex, *Chem. Eng. J.*, **309**: 80–88 (2017).

[35] Sostaric A., Stojic A., Stojic S., Grzeti I., Quantification and Mechanisms of BTEX Distribution Between Aqueous and Gaseous Phase in a Dynamic System, *Chemosphere*, **144**: 721-727 (2016).

[36] www.europarl.europa.eu

[37] Kim Y.N., Shao G.N., Jeon S.J., Imran S.M., Sarawade P.B., Kim H.T., Sol-Gel Synthesis of Sodium Silicate and Titanium Oxychloride Based TiO_2–SiO_2 Aerogels and their Photocatalytic Property under UV Irradiation, *Chem. Eng. J.*, **231**: 502–511 (2013).

[38] Yu Y., Zhu M., Liang W., Rhodes S., Fang J., Synthesis of Silica-Titania Composite Aerogel Beads for the Removal of Rhodamine B in Water, *RSC Adv*., **5**: 72437-72443 (2015).

[39] www.preview-nanoscalereslett.springeropen.com

[40] Munir Sh., Shah S.M., Hussain H., Ali khan R., Effect of Carrier Concentration on the Optical Band Gap of TiO_2 Nanoparticles, *Mater. Des.*, **92**: 64–72 (2016).

[41] Chan Wai S., Ching Juan J., Wei Lai Ch., Bee Abd Hamid Sh., Yusop R.M., Fe-doped Mesoporous Anatase-Brookite Titania in the Solar-Light-Induced Photodegradation of Reactive Black 5 Dye, *J. Taiwan. Inst. Chem. Eng.*, **68**: 153-161 (2016).

[42] Shamsa M., Shah S.M., Hussain H., Ali khan R., Effect of Carrier Concentration on the Optical Band Gap of TiO_2 Nanoparticles, *Mater. Des.*, **92**: 64-72 (2016).

[43] Kittel C., "Introduction to Solid State Physics", John Wiley & Sons, Inc., (2005).

[44] Bensouici F., Bououdina M., Dakhel A.A., Tala-Ighil R., Tounane M., Iratni A., Souier T., Liu S., Cai W., Optical, structural and Photocatalysis Properties of Cu-Doped TiO_2 Thin Films, *Appl. Surf. Sci.*, **395**: 110–116 (2017).

[45] Valentin C.D., Pacchioni G., Selloni A., Origin of the Different Photoactivity of N-Doped Anatase and Rutile TiO_2, *Phys. Rev. B.*, **70**: 085116 (2004).

[46] Vittoria Dozzi M., Selli E., Doping TiO_2 with p-block Elements: Effects on Photocatalytic Activity, *J. Photochem. Photobiol. C.*, **14 (1)**: 13-28 (2013).

[47] Senthilnathan J., Photodegradation of Methyl Parathion and Dichlorvos from Drinking Water with N-Doped TiO_2 Under Solar Radiation, *Chem. Eng. J.*, **172 (2)**: 678-688 (2011).

[48] Senthilnathan J., Philip L., Photocatalytic Degradation of Lindane under UV and Visible Light Using N-Doped TiO_2, *Chem. Eng. J.*,**161**: 83–92 (2010).

[49] Wei W., Lü X., Jiang D., Zaoxue Y., Chen M., Xie J., A Novel Route for Synthesis Of UV-resistant Hydrophobic Titania-Containing Silica Aerogels by Using Potassium Titanate as Precursor, *Dalton Trans*., **43**: 9456 (2014).

[50] Hongquan J., Wang Q., Zang Sh., Li J., Wang Q., Enhanced Photoactivity of Sm, N, P-Tridoped Anatase-TiO_2 Nano-Photocatalyst for 4-Chlorophenol Degradation inder Sunlight Irradiation, *J. Hazard. Mater.*, **261**: 44-54 (2013).

[51] Colon G., Maicu M., Hidalgo M.C., Navio J.A., Cu-Doped TiO_2 Systems with Improved Photocatalytic Activity, *Appl. Catal. B.*, **67**: 41-51 (2006).

[52] Xia X., Gao Y., Wang Z., Jia Z.J., Structure and Photocatalytic Properties Of Copper-Doped Rutile, TiO_2 Prepared by a Low-Temperature Process, *J. Phys. Chem. Solids.*, **69**: 2888–2893 (2008).

[53] Yadav M., Otari V., Koli B., Mali S., Hong Ch.K., Pawar H., Delekar D., Preparation and Characterization of Copper-Doped Anatase TiO_2 Nanoparticles with Visible Light Photocatalytic Antibacterial Activity, *J. Photochem. Photobio.l A.*, **280**: 32–38 (2014).

[54] Li Z.D., Wang H.L., Wei X.N., Liu X.Y., Yang Y.F., Jiang W.F., Preparation and Photocatalytic Performance of Magnetic Fe_3O_4@TiO_2 core-Shell Microspheres Supported by Silica Aerogels from Industrial Fly Ash, *J. Alloys. Compd.*, **659**: 240-247 (2016).

[55] Wang X., Liu J., Liu S., Feng X., Bao L., Shi F., Influences of Heat-Treatment on the Microstructure And Properties of Silica–Titania Composite Aerogels, *J. Porous. Mater.*, **21**: 293–301 (2014).

[56] Kannaiyan D., Kochuveedu S.Th., Jang Y.H., Jang Y.J., Enhanced Photophysical Properties of Nanopatterned Titania Nanodots/Nanowires upon Hybridization with Silica via Block Copolymer Templated Sol-Gel Process, *Polymers*, **2**: 490-504 (2010).

[57] Tang R., Chen T., Chen Y., Zhang Y., Wang G., Core-Shell TiO_2@SiO_2 Catalyst for Transesterification of Dimethyl Carbonate and Phenol to Diphenyl Carbonate, *Chin. J. Catal.*, **35**: 457–461 (2014).

[58] Bethi B., Sonawane Sh.H., Bhanvase B.A., Gumfekar S.P., Nanomaterials-Based Advanced Oxidation Processes for Wastewater Treatment, *Chem. Eng. Process.*,**109**: 178-189 (2016).

[59] www.article.sapub.org.

[60] Sarawade P., Kim J.K., Hilonga A., Hee T., Production of Low-Density Sodium silicate-based Hydrophobic Silica Aerogel Beads by a Novel Fast Gelation Process and Ambient Pressure Drying Process, *Solid State Sci.*, **12**: 911–918 (2010).

[61] Sahu M., Biswas P., Single-Step Processing of Copper-Doped Titania Nanomaterials in a Flame Aerosol Reactor, *Nanoscale Res. Lett.*, **6**: 441 (2011).

[62] Zhang Z., Wang Ch.Ch., Zakaria R., Ying J., Role of Particle Size in Nanocrystalline TiO_2-Based Photocatalysts, *J. Phys. Chem. B.*,**102**: 10871-10878 (1998).

[63] Ouidri S., Khalaf H., Synthesis of Benzaldehyde from Toluene by a Photocatalytic Oxidation Using TiO_2-Pillared Clays, *J. Photoch. Photobio. A.*, **207**: 268–273 (2009).

[64] Shinde S.S., Bhosale C.H., Rajpure K.Y., Photocatalytic Degradation of Toluene Using Sprayed N-Doped ZnO Thin Films in Aqueous Suspension, *J. Photoch. Photobio. B.*, **113**: 70–77 (2012).

[65] Bianchi C.L., Gatto S., Pirola C., Naldoni A., Di Michele A., Cerrato G., Crocellà V., Capucci V., Photocatalytic Degradation of Acetone, Acetaldehyde and Toluene in Gas-Phase: Comparison Between Nano and Micro-Sized TiO_2, *Appl. Catal. B.*, **146**: 123– 130 (2014).